

Synthesis and Characterization of High Temperature Properties of $\text{YBa}_2\text{Cu}_3\text{O}_{6+\delta}$ Superconductor as Potential Cathode for Intermediate Temperature Solid Oxide Fuel Cells

Joaquín Grassi¹, Mario A. Macías^{1,2}, Juan F. Basbus³, Jorge Castiglioni⁴, Gilles H. Gauthier⁵, Adriana C. Serquis³ and Leopoldo Suescun^{1,*}

¹*Cryssmat-Lab/DETEMA, Facultad de Química, Universidad de la República, Montevideo, Uruguay*

²*Departamento de Química, Universidad de los Andes, Carrera 1 No 18A-12, Bogotá, Colombia*

³*Departamento de Caracterización de Materiales, CAB-INN-CNEA-CONICET, Av. Bustillo 9500, San Carlos de Bariloche, Rio Negro (8400), Argentina*

⁴*Área de Fisicoquímica/DETEMA, Facultad de Química, Universidad de la República, Montevideo, Uruguay*

⁵*Universidad Industrial de Santander, INTERFASE, Bucaramanga, Colombia*

Abstract: $\text{YBa}_2\text{Cu}_3\text{O}_{6+\delta}$ (YBC) oxygen deficient perovskite was synthesized by an auto-combustion method and was studied as potential cathode for Intermediate Temperature Solid Oxide Fuel Cell (IT-SOFC). Synchrotron X-ray thermofraction in air shows a phase transition from orthorhombic $Pmmm$ to tetragonal $P4/mmm$ space groups at ~ 425 °C. The chemical compatibility with $\text{Ce}_{0.9}\text{Gd}_{0.1}\text{O}_{1.95}$ (GDC) electrolyte was investigated in air where certain reactivity was observed above 800 °C. However, the main phase is $\text{Ba}(\text{Ce}_{1-x}\text{Y}_x)\text{O}_3$, a good ionic conductor. The catalytic performance in air was obtained by electrochemical impedance spectroscopy (EIS) measurements on YBC/GDC/YBC symmetrical cells. The area specific resistance (ASR) values change from 13.66 to 0.14 $\Omega \text{ cm}^2$ between 500 and 800 °C, with activation energy (E_a) of 0.41 eV. The results suggest potential applications of YBC as IT-SOFC cathode.

Keywords: $\text{YBa}_2\text{Cu}_3\text{O}_{6+\delta}$ perovskite, IT-SOFC, Cathode, Auto-combustion synthesis, Electrochemical performance.

1. INTRODUCTION

Solid Oxide Fuel Cells (SOFCs) are considered an excellent alternative among the different sources of clean energy, due to its demonstrated efficiency, fuel flexibility and long term stability [1]. Currently, the interest in those devices is focused especially in the intermediate temperature SOFCs (IT-SOFC) that operate between 600 and 800 °C, increasing cell durability and allowing for the use of cheaper interconnect and support materials. However, these features create the necessity for new materials with sufficient electrochemical activity in this range of temperature besides chemical and thermomechanical stability. Some cobalt-based oxides with perovskite or perovskite-derived structure, such as $\text{A}_x\text{A}'_{1-x}\text{CoO}_{3-\delta}$ ($\text{A} = \text{Ln}, \text{Y}; \text{A}' = \text{alkaline earths}; x \geq 0.5$) [2, 3], $\text{Ba}_{0.5}\text{Sr}_{0.5}\text{Co}_{0.8}\text{Fe}_{0.2}\text{O}_{3-\delta}$ [4] and $\text{AA}'\text{Co}_2\text{O}_{5+\delta}$ [5, 6] are currently studied as new cathodes for IT-SOFC due to their mixed ionic electronic conductivity (MIEC) and good oxygen reduction reaction (ORR) catalytic properties. Nevertheless, those Cobalt-based

compounds present drawbacks due to high chemical reactivity with the available electrolytes and high thermal expansion coefficients [7], among others. In the investigation for new cobalt-free materials, promising properties have been observed in some compounds such as $\text{Sm}_{0.5}\text{Sr}_{0.5}\text{Fe}_{0.8}\text{Cu}_{0.2}\text{O}_{3-\delta}$ [8], $\text{Ba}_{0.5}\text{Sr}_{0.5}\text{Fe}_{0.8}\text{Cu}_{0.2}\text{O}_{3-\delta}$ [9], $\text{La}_{0.6}\text{Sr}_{0.4}\text{Fe}_{0.8}\text{Cu}_{0.2}\text{O}_{3-\delta}$ [10, 11], $\text{La}_{1-x}\text{Sr}_x\text{CuO}_{2.5-\delta}$ ($0.1 < x < 0.5$) [12], $\text{La}_4\text{BaCu}_5\text{O}_{13+\delta}$ and $\text{La}_{6.4}\text{Sr}_{1.6}\text{Cu}_8\text{O}_{20+\delta}$ [13] perovskites.

This search for new cathodes inspired us to study conventional copper oxides, for which promising perspectives were observed [13]. Following this idea, we engaged to study the traditional superconductor $\text{YBa}_2\text{Cu}_3\text{O}_7$ (YBCO123 or simply YBC) as potential cathode for IT-SOFCs. This material shows a significant number of mobile vacancies at low temperatures and, depending on the doping level, it is metallic or semiconducting allowing for MIEC activity. In addition, we expect to contribute to the knowledge of the material's behavior at high temperatures, since reports on the study of the oxygen mobility associated to conductivity properties in this compound above 500 °C are very scarce [14]. To the best of our knowledge, the potential use of superconducting cuprates as SOFC electrode materials had been reported only for

*Address correspondence to this author at the Cryssmat-Lab/DETEMA, Facultad de Química, Universidad de la República, Montevideo, Uruguay; Tel: +598 29290705; E-mail: leopoldo@fq.edu.uy

$\text{YSr}_2\text{Cu}_2\text{MO}_{7+\delta}$, (M = Co, Fe) compounds [15, 16]. Very recently this approach to the use of cuprates has also been employed in the preparation and testing of $\text{PrBa}_{2-x}\text{Sr}_x\text{Cu}_3\text{O}_{6+\delta}$ as an IT-SOFC cathode [17]. In this work, $\text{YBa}_2\text{Cu}_3\text{O}_{6+\delta}$ (YBC) powders were obtained through an auto-combustion reaction path and were characterized by X-ray diffraction (XRD) between room temperature (RT) and 700 °C to confirm phase formation and transformations and determine thermomechanical and chemical compatibility with $\text{Ce}_{0.9}\text{Gd}_{0.1}\text{O}_{1.95}$ (GDC) electrolyte material. Thermogravimetric (TG) measurements were performed to confirm oxygen sorption at high temperatures. YBC/GDC/YBC symmetric cells were obtained and characterized by Scanning Electron Microscopy (SEM) and Electrochemical Impedance Spectroscopy (EIS) to determine morphology and thickness of the electrode and calculate the polarization resistance values, respectively.

2. EXPERIMENTAL

2.1. Synthesis, Crystallographic Analysis and Study of Thermodynamical Properties

$\text{YBa}_2\text{Cu}_3\text{O}_{6+\delta}$ (YBC) was synthesized using an auto-combustion method, which allowed us the preparation of a microstructured material, suitable for application as cathodes in SOFCs, at about 850 °C in a few hours [9, 11]. Stoichiometric amounts of $\text{Y}(\text{NO}_3)_3 \cdot 6\text{H}_2\text{O}$ (Sigma-Aldrich 99.8 %), $\text{Ba}(\text{NO}_3)_2$ (Sigma-Aldrich ≥ 99 %) and $\text{Cu}[\text{CH}_3\text{COO}]_2 \cdot \text{H}_2\text{O}$ (Sigma-Aldrich ≥ 99.0 %) were dissolved in distilled water and magnetically stirred at room temperature until an homogeneous solution was observed. After the dissolution step, EDTA (ethylenediaminetetraacetic acid, Sigma-Aldrich ≥ 99.4 %) was added as chelating agent in a molar ratio of $\text{EDTA}:(\text{metal})_{\text{total}} = 1.1:1$ using NH_4OH (Sigma-Aldrich 28.0-30.0 %) which was regularly poured in drops to keep the pH value between 9 and 10 and avoid precipitation of metals. The resulting blue solution was heated at 80 °C using a hot plate and ethylene glycol was added in a proportion of 1.5 mL per gram of final targeted product. The solution was subsequently evaporated at about 100-120 °C until a clear blue gel was formed which was kept under magnetic stirring of ~ 100 rpm until a solid blue product was formed as result of the complete solvent evaporation. The gel was burned directly in the beaker over the hot plate at ~ 250 °C to form foam-like ashes and subsequently the temperature was raised to ~ 500 °C for about 30 min in order to complete the organic matter decomposition.

The resulting product was ground in an agate mortar, pressed into pellets and then calcined at 850 °C in air for 16 hours with one intermediate grinding to ensure a correct homogeneity of the sample. Since no change was observed in the resulting sample between the first and second firing step, one calcination at 850 °C for 12 hours in air was used for the samples characterized in this study.

Laboratory X-ray diffraction (XRD) patterns were recorded to characterize the YBC compound and study the cathode-electrolyte chemical compatibility. For this purpose, a Rigaku ULTIMA IV powder diffractometer was used, operating at 40 kV/30 mA using $\text{CuK}\alpha_{1,2}$ radiation ($\lambda_{\text{ave}} = 1.5418$ Å) in a θ - θ Bragg-Brentano geometry. The patterns were collected using a 2 θ step size of 0.02 ° in the 2 θ range of 10-70 ° for the chemical compatibility studies and in the 2 θ range of 6-100 ° for Rietveld analysis of the pure YBC sample performed using the Jana-2006 program [18]. Synchrotron X-ray diffraction (S-XRD) patterns were also collected over YBC sample at D10B-XPD beamline of the UVX ring of the Brazilian Synchrotron Light Laboratory. The diffractometer was set in θ -2 θ mode with the sample mounted on a flat, rotating sample holder inserted in an ARARA Furnace [19] working with dry-air flow and a Mythen 1000 linear detector in the 2 θ arm at 1050 mm from the sample. The detector spanned ~3.6 ° in 2 θ in such conditions. Radiation energy was selected to be approximately 10 keV and the wavelength was determined by Rietveld fit of a Y_2O_3 powder standard sample ($\lambda = 1.2385(1)$ Å). Full patterns were collected in the 2 θ range 10 – 120 ° in 0.5 ° steps. Data was re-binned to a 2 θ -step of 0.005 ° with seven detector passes contributing to each point. In addition to room temperature, the temperature range selected for Rietveld analysis was from 350 to 700 °C on heating. Also, a series of short patterns were collected with the detector fixed at 2 $\theta = 25.9$ °, collecting data in the range 24.4 – 27.0 ° (2 θ) every minute and at constant cooling rate of 3 °C.min⁻¹ from 600 to 300 °C. The patterns collected on heating run were fitted with the GSAS/EXPGUI suite of programs [20, 21] while the thermodiffraction data was visualized using Origin 8. The evolution of cell parameters with temperature allowed to determine the crystallographic thermal expansion coefficients (TEC) and phase transition temperature.

Thermogravimetric (TG) analysis was performed using a Shimadzu TGA-50 in synthetic air (20 % O_2 ; 80 % N_2) in order to study the oxygen exchange as a function of temperature. The sample weight was

measured in a gas flow of 50 mL min^{-1} and a platinum capsule as sample holder between room temperature (RT) and $900 \text{ }^\circ\text{C}$ with a heating ramp of $5 \text{ }^\circ\text{C min}^{-1}$. In addition, complementary TG measurement was performed in pure oxygen flow to estimate oxygen content in synthetic air (see Supplementary Information).

2.2. Preparation of Symmetrical Cells and Characterization in Air

In order to prepare symmetric cells for Electrochemical Impedance Spectroscopy (EIS) measurements, we followed the procedure described in [22]. The electrodes were prepared as ink and deposited by spin-coating method on dense pellets of $\text{Ce}_{0.9}\text{Gd}_{0.1}\text{O}_{1.95}$ (GDC) electrolyte, preliminarily sintered at $1300 \text{ }^\circ\text{C}$; a rotation speed of about 4000 rpm was used for ~ 20 seconds forming a layer of uniform thickness. The ink was prepared by mixing the sample with α -terpineol (Alfa Aesar 96%), polyvinylpyrrolidone (Alfa Aesar M.W. 8k), poly(vinyl butyral-co-vinyl alcohol-co-vinyl acetate) (Sigma Aldrich M.W. 50k-80k) and isopropanol (Sigma Aldrich $\geq 99.5\%$) in amounts of 35 %, 22 %, 1 %, 2 % and 40 % in weight, respectively. Two layers of the as prepared ink were deposited on each side of the electrolyte dense pellet. After each layer deposition, the cell was dried at $150 \text{ }^\circ\text{C}$ for 10 min and subsequently sintered at $900 \text{ }^\circ\text{C}$ for 1 hour to achieve a correct electrode/electrolyte adhesion. The sample was characterized by high resolution Scanning Electron Microscopy (SEM) using a field emission gun (FEG) FEI Nova NanoSEM 230 to determine the thickness of the deposited electrodes as well as the layer uniformity. In addition, the microscope is equipped with Energy Dispersive Spectroscopy (EDS) detector for elementary analysis.

The chemical reactivity between YBC cathode and GDC electrolyte powders was studied weighing equal masses of each phase (*i.e.*, 1:1 mass ratio of YBC/GDC), grinding and pressing into a pellet before firing at 650 , 750 or $850 \text{ }^\circ\text{C}$ in air for 6 hours. The results were analyzed by XRD using ICDD-PDF2 (2013) database running on Crystallographica Search Match Software (Oxford cryosystems) for phase identification.

The area-specific resistance (ASR) values of the prepared symmetrical cell were determined from EIS measurements in air flow between 500 and $800 \text{ }^\circ\text{C}$ using heating steps of $50 \text{ }^\circ\text{C}$, collecting data on heating and cooling to verify the stability of the cell. The EIS

measurements were performed using a potentiostat/impedance analyzer Autolab PGSTAT30 potentiostat/galvanostat between 1 mHz and 1MHz with an amplitude of 100 mV . The data collection was carried out using platinum grids pressed on the porous electrodes as current collectors and average dwell times of 3 hours to reach equilibrium as reported in [23]. The electrode polarization resistance values for each temperature were calculated using the ZView3.0 software, fitting the spectra with equivalent electric circuits (EEC). The spectra were fitted by series circuits of R_s - W -(R // CPE) for the whole temperature, where R_s , W and R // CPE corresponds to the electrolyte ohmic resistance, Warburg element and resistance in parallel with a constant phase element, respectively. According to bibliography, R // CPE and W corresponds to the charge transfer and oxygen diffusion resistances, respectively [24, 25].

3. RESULTS AND DISCUSSION

3.1. Structural and Thermal Analysis

XRD analysis confirmed that YBC was successfully obtained by the auto-combustion method that has the advantage of being a relatively simple, quick and straightforward preparation process, suitable for obtaining fine-grained samples with high particle size homogeneity, a desirable feature for SOFCs applications.

Figure 1 shows the refinement and the structural model of the YBC powder sample and Table 1 summarizes crystallographic information and goodness of fit. The structural analysis using the Rietveld method showed that YBC crystallizes in the orthorhombic $Pmmm$ space group. Despite the excellent results obtained from this synthetic method, it was not possible to avoid the formation of BaCuO_2 [26-28] (less than 1 wt. % according to the Rietveld refinement). The refined structure (see Table 1) is in agreement with the structure solved using neutron diffraction [29]. The description of the oxygen vacancies was performed following this model which proposes that all of them are concentrated in the O1 site with Wyckoff position 1e at (0,1/2,0).

Refinements were performed leaving the O2, O3 and O4 sites fixed to full occupancy and refining only the occupancy parameter of the O1 site. The standard deviation value obtained for the site occupancy was relatively high (0.82 ± 0.35), compared with the refined parameter itself. We attempted to use Benzi's equation that relates the oxygen content with the c -axis of the

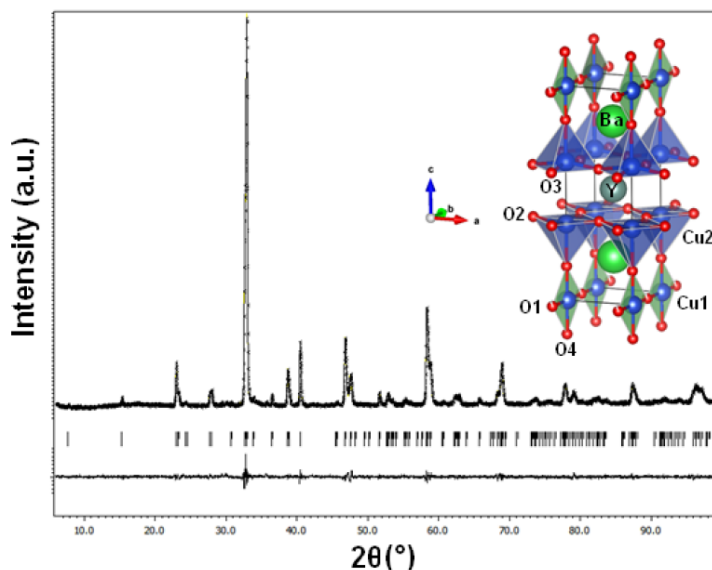


Figure 1: Rietveld fit for YBC compound using the conventional XRD data.

Table 1: Crystal Structure Parameters for YBC Compound Obtained for YBC Sample Prepared by Auto-Combustion Method after Rietveld Refinement using XRD Data

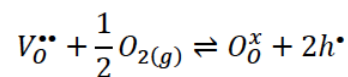
Atom	Site	x	y	z	$U_{iso} (\text{Å}^2)$	Occupancy
Y1	1h	1/2	1/2	1/2	0.0049(8)	1.0
Ba1	2t	1/2	1/2	0.1845(3)	0.0049(8)	1.0
Cu1	1a	0	0	0	0.0132(16)	1.0
Cu2	2q	0	0	0.3559(7)	0.0132(16)	1.0
O1	1e	0	1/2	0	0.012(5)	0.82
O2	2s	0	1/2	0.377(3)		1.0
O3	2r	1/2	0	0.374(3)		1.0
O4	2q	0	1/2	0.145(3)		1.0

Lattice Parameters: $a = 3.8339(3) \text{ Å}$, $b = 3.8862(5) \text{ Å}$, $c = 11.6675(14) \text{ Å}$,
 Space Group: $Pmmm$ (N° 47).
 $R_p = 4.64$, $R_{wp} = 6.27$, $\chi^2 = 1.56$

unit cell of YBC [30] to determine the number of oxygen vacancies. The calculated value of 0.91 is however inconsistent with the TG results (since the oxygen content of O_2 cooled sample would be larger than 7). New refinements were performed using a fixed value of 0.82 for O1 site occupancy (for a starting composition $YBa_2Cu_3O_{6.82}$). The R -factors seem not to be affected considerably by the variation of this parameter (see Table 1).

Figure 2 shows the TG measurements for YBC sample. The material exhibits an oxygen uptake on heating in air from RT up to $\sim 400 \text{ °C}$, from which it starts losing oxygen, until the maximum temperature is reached (900 °C). On cooling, the sample absorbs

oxygen and gains weight until the maximum oxygen content is reached (again around $\sim 400 \text{ °C}$), but further cooling does not reproduce the heating behavior, with the observation of a constant oxygen content for the duration of the cooling process. This mass gain is due to the fact that the orthorhombic phase at room temperature shows non-null oxygen vacancy concentration. The process can be represented by the following equation, using the Kröger-Vink notation:



where $V_o^{\bullet\bullet}$, O_o^x and h^{\bullet} corresponds to oxygen vacancies, oxygen sites and holes, respectively. The

occupation of V_O^\bullet sites produce the oxidation of Cu^+ (at 1a crystallographic site) to Cu^{3+} with an increase in the holes' concentration, favoring the *p-type* conductivity processes for temperatures below 400 °C. At temperatures above 400 °C the loss of oxygen observed causes the reduction from Cu^{3+} to Cu^+ ; this phenomenon suggests a variation in the electronic behavior of the material presenting a semiconductor and metallic character below and above 400 °C, respectively, as described in [23].

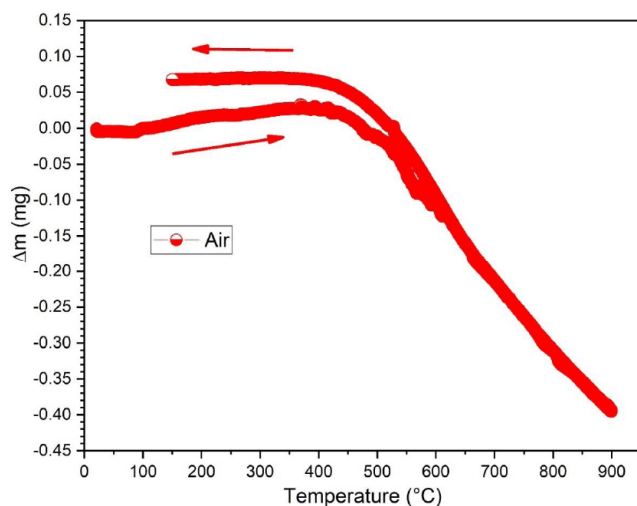


Figure 2: TGA curve in synthetic air of YBC powder.

The hysteresis observed in the curve indicates that non-stoichiometry ($6+\delta$) is constant below 400 °C. This suggests that both the exchange and the mobility of oxygen within the structure will be a very slow process at low temperature. Such phenomenon could be related to the structure change of YBC and vacancies mobility in the material as a function of temperature, as discussed in the next sections.

Figure 3 shows the evolution with temperature of the cell parameters of YBC in air, as determined from the Rietveld fits. The results show that YBC presents an orthorhombic *Pmmm* to tetragonal *P4/mmm* phase transition during heating between 450 and 500 °C. Figure 4 shows the evolution of the main diffraction peaks of YBC from 600 to 300 °C on cooling, where a clear peak splitting is observed at 425(5) °C corresponding to the reverse phase transition from the tetragonal to the orthorhombic forms. The oxygen vacancy-ordered orthorhombic phase gives place to a disordered tetragonal phase, where O1 oxygen in (0,1/2,0) position, in the basal plane of the orthorhombic cell, is disordered over (1/2,0,0) and (0,1/2,0) sites in the tetragonal cell. Such behavior was already described by Jorgensen *et al.* [31] as an

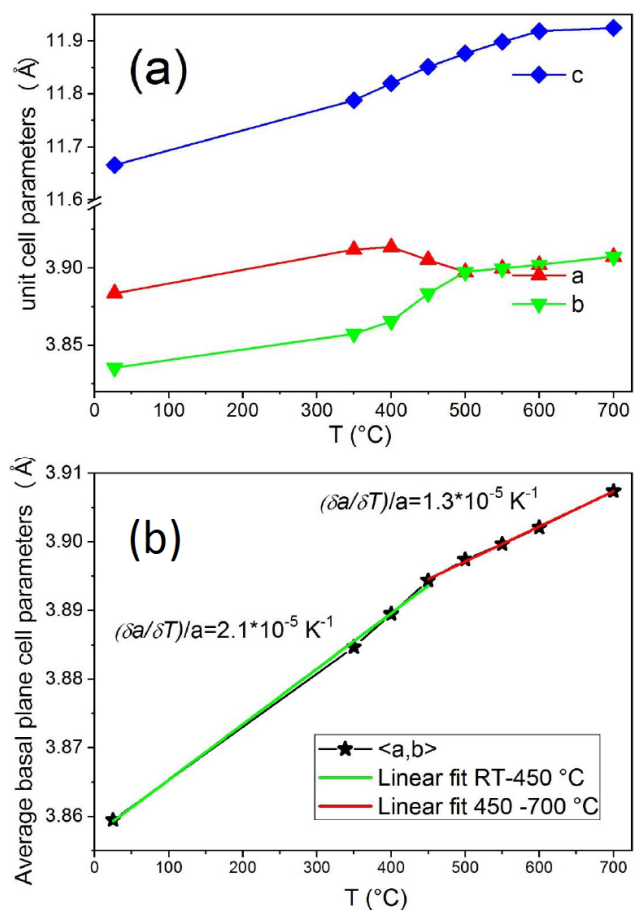


Figure 3: a) Evolution of lattice parameters as a function of temperature in air, where the phase transition occurs at ~ 425 °C. b) Fit of the evolution of $\langle a,b \rangle$ parameters with temperature with associated coefficient of linear expansion.

oxygen-vacancy order-disorder phase transition. Jorgensen and other authors [31-33] investigated $\text{YBa}_2\text{Cu}_3\text{O}_{6+\delta}$ sample annealed at or above 900 °C demonstrating that oxygen partial pressure affects the transition temperature. It has been suggested that the phase transition is related to the oxygen content of the sample with the orthorhombic phase dominating at $\delta > 0.5$ while the tetragonal phase showing at $\delta < 0.5$. Misuzaki *et al.* [34] showed the *Pmmm* to *P4/mmm* phase transition temperature to occur at a temperature of as low as 435 °C on heating. The phase transition temperature we observe is lower than reported at $p\text{O}_2 \sim 0.2$ (air) around 620 °C for YBC (or ~ 550 °C for related $\text{LnBa}_2\text{Cu}_3\text{O}_{6+\delta}$ compounds [24]), but we have a smaller particle size since our samples were prepared at 850 °C. We expect this plays an important role in the oxygen-exchange and the associated structure. The oxygen-vacancy order-disorder phase transition is expected to complete above 500 °C in our case, as observed by EIS measurements and discussed below.

Some hysteresis is observed in the X-ray diffraction data, since the phase transition temperature is higher on heating than on cooling. This is probably associated with the no-equilibrium of the oxygen content of the sample associated with the high cooling rate of the experiment.

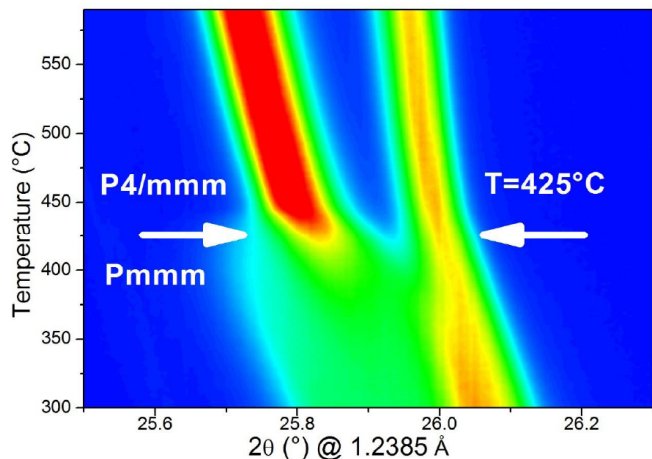


Figure 4: Thermo diffraction data showing the evolution in air of the main diffraction peaks of YBC phase with temperature from high to low temperature: Tetragonal $103/110$ doublet (top) and Orthorhombic $103/013/110$ triplet (low temperature). The phase transition at $\sim 425^\circ\text{C}$ is indicated.

This change in symmetry also coincides with the maximum of oxygen content and beginning of the hysteresis on cooling shown in the TG line (Figure 2). This is more evident if we consider that, on cooling, the oxygen content of YBC remains constant below the phase transition [24], suggesting that the lower temperature and vacancy-ordering makes the sample a poorer ionic conductor.

It has been reported that oxygen-annealed $\text{YBa}_2\text{Cu}_3\text{O}_7$ powders or pellets showing superconductivity above liquid nitrogen (LN) temperature (77 K), slowly lose O_2 at room temperature [35]. This process makes $\text{YBa}_2\text{Cu}_3\text{O}_{6+\delta}$ with a critical temperature (T_c) below N_2 boiling point, requiring a new annealing in O_2 to recover high- T_c superconductivity. This explains why the oxygen content of starting YBC samples ($\delta \approx 0.82$), from a sample prepared at 850°C and slowly cooled and stored in air for several weeks, was lower than the final oxygen content on cooling run during the TG experiment. Assuming that the oxygen content of the initial sample at RT is 0.82, the estimated oxygen content of a sample slowly cooled in air would be 0.88 and the same sample further cycled in O_2 would have an oxygen content of $\delta=0.95$ consistent with previous reports [31] (see Figure S1 where TGA of the sample in pure O_2 is shown).

In addition, the crystallographic thermal expansion coefficient (TEC) of YBC was determined in the temperature range of interest by fitting the unit cell parameters obtained by the Rietveld method. As expected for a layered compound, the TEC of the unit cell is very anisotropic with c lattice parameter increasing at a rate 2-3 times faster than a/b . The average TEC computed as $\langle \text{TEC} \rangle = (2\text{TEC}_{ab} + \text{TEC}_c)/3$ shows values of $2.6 \times 10^{-5} \text{ K}^{-1}$ and $2.0 \times 10^{-5} \text{ K}^{-1}$ below and above the phase transition respectively and 3.6×10^{-5} for TEC_c in the same temperature interval. This change in TEC is caused by a significant change in the structure of oxygen vacancies in the a - b plane. The TEC values calculated for YBC are different from those of the TEC for conventional electrolytes, but their magnitude is within the ranges reported for cathodes and electrolytes used for IT-SOFC [25]. In case of electrode layer delamination, such TEC mismatch could be mitigated by the use of YBC/GDC graded electrodes.

3.2. Preparation and Performance of a Symmetric Cell

In order to evaluate properly the YBC/GDC reactivity at high temperature, chemical compatibility tests were performed at 650 , 750 and 850°C for 6 hours in air. As shown in Figure 5, at 650 and 750°C , both phases remain unchanged and no extra peaks appear. However, at 850°C , extra peaks are observed which can be explained by the occurrence of a cubic phase that corresponds to the $\text{Ba}(\text{Ce}_{1-x}\text{Y}_x)\text{O}_{3-\delta}$ series (possibly doped with Gd).

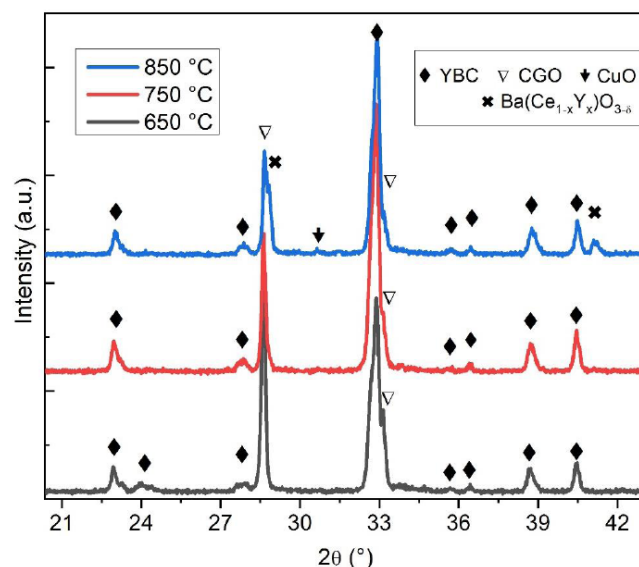


Figure 5: RT XRD patterns after reactivity tests between YBC and GDC powders in air.

Figure 6 presents SEM images of the YBC/GDC/YBC symmetric cell. The porous electrode can be clearly observed with an average thickness of $\sim 24 \mu\text{m}$ and individual particle size estimated to be well below $1 \mu\text{m}$. This small particle size for YBC has only been reported by Xu *et al.* [26] in samples prepared by sol-gel and annealed as a loose powder at $880 \text{ }^\circ\text{C}$, similar to our cathode preparation conditions. Considering the temperature of electrode sintering, a careful study of the interfacial region between the electrode and the dense electrolyte has been carried out, which does not reveal any formation of an interlayer phase of $\text{Ba}(\text{Ce}_{1-x}\text{Y}_x)\text{O}_{3-\delta}$. However, in case it is present as very thin layer, it would perhaps not be completely detrimental to the cell performance [36, 37], as this phase may act as an interlayer reducing the TEC mismatch between YBC and GDC [38, 39]. Otherwise, the pellet shows neither micro-fractures nor

damaged boundaries suggesting a reasonable electrode/electrolyte adhesion.

In order to investigate the potential use of YBC as cathode for IT-SOFCs, the electrochemical response of the electrodes was analyzed by EIS. The YBC/GDC/YBC symmetrical cells were studied as a function of temperature in air flow. The electrode polarization resistances were calculated from the fit using an EEC of the experimental data (Table S1).

The catalytic performance of the electrode was calculated by the area specific resistance: $ASR = R_{el} \cdot S/2$ where R_{el} and S correspond to the polarization resistance from impedance spectra fit and normalized area of the pellet, respectively. Figure 7a shows the impedance spectrum and fit at $500 \text{ }^\circ\text{C}$. The Nyquist plots show two typical arcs, one corresponding to low

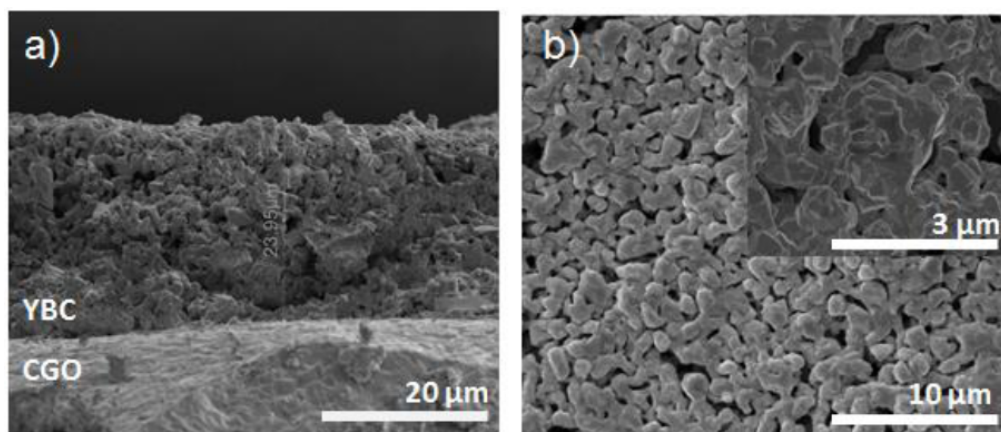


Figure 6: SEM images of a) the cross-section of YBC layer deposited on GDC and b) the top of the corresponding YBC electrode surface.

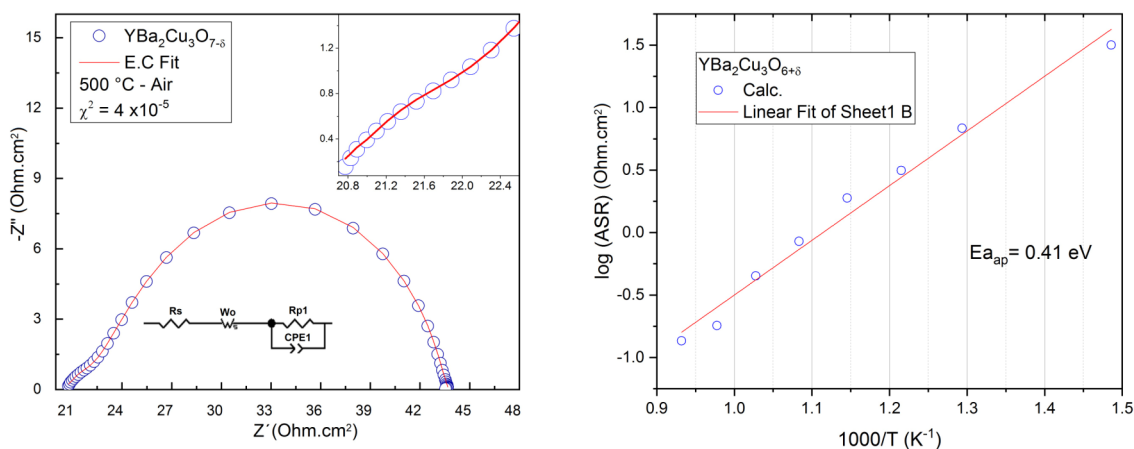


Figure 7: a) Fit of the impedance spectrum of YBC/GDC/YBC symmetrical cell measured at $500 \text{ }^\circ\text{C}$ in air; b) Arrhenius plot of ASR between 500 and $800 \text{ }^\circ\text{C}$.

and the other to high frequencies in the whole temperature range. Figure 7b shows the Arrhenius plot of the total ASR where the values change from $13.66 \Omega \text{ cm}^2$ at 500°C to $0.14 \Omega \text{ cm}^2$ at 800°C with an activation energy $E_a = 0.41 \text{ eV}$. These values are larger than observed in materials such as $\text{Ba}_{0.5}\text{Sr}_{0.5}\text{Fe}_{0.8}\text{Cu}_{0.2}\text{O}_{3-\delta}$ with ASR value of $0.033 \Omega \text{ cm}^2$ at 700°C [9], but are close to other compounds proposed as IT-SOFC cathodes such as the barium deficient $\text{NdBa}_{1-x}\text{Co}_2\text{O}_{5+\delta}$ with ASR values of $0.1\text{-}0.99 \Omega \text{ cm}^2$ at 700°C [40].

4. CONCLUSIONS

We have prepared $\text{YBa}_2\text{Cu}_3\text{O}_{6+\delta}$ perovskite oxide through an auto-combustion procedure obtaining the material at a low temperature of 850°C with a very low degree of impurities. We studied the sample at high temperatures with the aim to use it as cathode for IT-SOFC with Gd-doped Ceria electrolyte. YBC shows a phase change from orthorhombic $Pmmm$ low temperature phase to tetragonal $P4/mmm$ high temperature phase between 425 and 500°C . A consequence of such transition from oxygen vacancy order to disorder is accompanied by an apparent increase in oxygen mobility that justifies the good electrochemical behavior. Even though the material reacts with the electrolyte at the cell preparation temperature, the presence of doped barium cerate, as product of the reaction, seems not to be detrimental to the performance of the electrode material. The electrochemical performance of YBC/GDC/YBC symmetric cells shows an ASR value of $0.14 \Omega \text{ cm}^2$ at 800°C , comparable with other electrodes proposed for IT-SOFCs. YBC shows a high TEC that varies with temperature, which may preclude its use in a single-phase cathode with known electrolytes, especially for larger cells of commercial size; however, this study confirms there is some potential in this and related cuprates for high-temperature applications. Our results show the versatility of $\text{YBa}_2\text{Cu}_3\text{O}_{6+\delta}$ compound that is not only a high- T_c superconductor at low temperature but also a possible MIEC with reasonable electrocatalytic properties at high temperatures.

5. ACKNOWLEDGMENTS

This work was supported by Agencia Nacional de Investigación e Innovación (ANII) – Uruguay, through grant FSE_2013_10443 and FSE_2015_109493, PEDECIBA and Laboratorio Nacional de Luz Síncrotron (LNLS, Campinas, SP, Brazil) through a grant to perform research proposal XPD20160246 at D10B-XPD beamline. M.M. and J.G. also thanks ANII

for the postdoctoral and doctoral grants PD_NAC_2014_1_102409 and POS_NAC_2018_1_152154 respectively. We thank Manuel Corte from Departamento de Caracterización de Materiales (CAB-CNEA) for SEM images.

REFERENCES

- [1] Aldo da Rosa, Fundamentals of Renewable Energy, 3rd ed., Oxford, UK, 2013.
<https://doi.org/10.1016/B978-0-12-397219-4.00017-5>
- [2] A. Samson Nesaraj, I. Arul Raj, R. Pattabiraman, Preparation and characterization of ceria-based electrolytes for intermediate temperature solid oxide fuel cells (IT-SOFC), J. Iran. Chem. Soc 2010; 7: 564-584.
<https://doi.org/10.1007/BF03246044>
- [3] C. Lee, S.W. Baek, J. Bae, Cathodic behavior of $\text{La}_{0.8}\text{Sr}_{0.2}\text{Co}_{1-x}\text{Mn}_x\text{O}_{3-\delta}$ perovskite oxide on YSZ electrolyte for intermediate temperature-operating solid oxide fuel cells, Solid State Ionics 2008; 179: 1465-1469.
<https://doi.org/10.1016/j.ssi.2008.01.009>
- [4] Z. Shai, S.M. Hale, A high-performance cathode for the next generation of solid-oxide fuel cells, Nature 2004; 431: 170-174.
<https://doi.org/10.1038/nature02863>
- [5] K. Zhang, L. Ge, R. Ran, Z. Shao, S. Liu, Synthesis, characterization and evaluation of cation-ordered $\text{LnBaCo}_2\text{O}_{5+\delta}$ as materials of oxygen permeation membranes and cathodes of SOFCs, Acta Mater 2008; 56: 4876-4889.
<https://doi.org/10.1016/j.actamat.2008.06.004>
- [6] J.H. Kim, M. Cassidy, J.T.S. Irvine, J. Bae, Advanced Electrochemical Properties of $\text{LnBa}[\text{sub } 0.5]\text{Sr}[\text{sub } 0.5]\text{Co}[\text{sub } 2]\text{O}[\text{sub } 5+\delta]$ (Ln=Pr, Sm, and Gd) as Cathode Materials for IT-SOFC, J. Electrochem. Soc 2009; 156: B682.
<https://doi.org/10.1149/1.3110989>
- [7] J.L. Yu, Y.M. Yin, Z.F. Ma, Preparation and characterization of new cobalt-free cathode $\text{Pr}_{0.5}\text{Sr}_{0.5}\text{Fe}_{0.8}\text{Cu}_{0.2}\text{O}_{3-\delta}$ for IT-SOFC, Int. J. Hydrogen Energy 2013; 38: 10527-10533.
<https://doi.org/10.1016/j.ijhydene.2013.05.164>
- [8] Y. Ling, L. Zhao, B. Lin, Y. Dong, X. Zhang, G. Meng, X. Liu, Investigation of cobalt-free cathode material $\text{Sm}_{0.5}\text{Sr}_{0.5}\text{Fe}_{0.8}\text{Cu}_{0.2}\text{O}_{3-\delta}$ for intermediate temperature solid oxide fuel cell, Int. J. Hydrogen Energy 2010; 35: 6905-6910.
<https://doi.org/10.1016/j.ijhydene.2010.04.021>
- [9] S. Vázquez, J. Basbus, A.L. Soldati, F. Napolitano, A. Serquis, L. Suescun, Effect of the symmetric cell preparation temperature on the activity of $\text{Ba}_{0.5}\text{Sr}_{0.5}\text{Fe}_{0.8}\text{Cu}_{0.2}\text{O}_{3-\delta}$ as cathode for intermediate temperature Solid Oxide Fuel Cells, J. Power Sources 2015; 274: 318-323.
<https://doi.org/10.1016/j.jpowsour.2014.10.064>
- [10] Q. Zhou, L. Xu, Y. Guo, D. Jia, Y. Li, W.C.J. Wei, $\text{La}_{0.6}\text{Sr}_{0.4}\text{Fe}_{0.8}\text{Cu}_{0.2}\text{O}_{3-\delta}$ perovskite oxide as cathode for IT-SOFC, Int. J. Hydrogen Energy 2012; 37: 11963-11968.
<https://doi.org/10.1016/j.ijhydene.2012.05.114>
- [11] S. Vázquez, S. Davyt, J.F. Basbus, A.L. Soldati, A. Amaya, A. Serquis, R. Faccio, L. Suescun, Synthesis and characterization of $\text{La}_{0.6}\text{Sr}_{0.4}\text{Fe}_{0.8}\text{Cu}_{0.2}\text{O}_{3-\delta}$ oxide as cathode for Intermediate Temperature Solid Oxide Fuel Cells, J. Solid State Chem 2015; 228: 208-213.
<https://doi.org/10.1016/j.jssc.2015.04.044>
- [12] H.C. Yu, K.Z. Fung, Electrode properties of $\text{La}_{1-x}\text{Sr}_x\text{CuO}_{2.5-\delta}$ as new cathode materials for intermediate-temperature SOFCs, J. Power Sources 2004; 133: 162-168.
<https://doi.org/10.1016/j.jpowsour.2004.02.002>

- [13] MA. Macias, MV. Sandoval, NG. Martinez, S. Vázquez-Cuadriello, L. Suescun, P. Roussel, K. Świerczek, GH. Gauthier, Synthesis and preliminary study of $\text{La}_4\text{BaCu}_5\text{O}_{13+\delta}$ and $\text{La}_{6.4}\text{Sr}_{1.6}\text{Cu}_8\text{O}_{20\pm\delta}$ ordered perovskites as SOFC/PCFC electrode materials, *Solid State Ionics* 2016; 288: 68-75.
<https://doi.org/10.1016/j.ssi.2016.02.010>
- [14] EB. Mitberg, MV. Patrakeev, IA. Leonidov, AA. Lakhtin, VL. Kozhevnikov, KR. Poeppelmeier, High-temperature thermodynamics of oxygen equilibrium of solid solutions $\text{YBa}_2\text{Cu}_3-x\text{Zn}_x\text{O}_{6+\delta}$ with gas phase, *J. Alloys Compd.* 274 (1998) 98-102.
[https://doi.org/10.1016/S0925-8388\(98\)00577-5](https://doi.org/10.1016/S0925-8388(98)00577-5)
- [15] JEH. Sansom, E. Kendrick, HA. Rudge-Pickard, MS. Islam, AJ. Wright, PR. Slater, Synthesis and characterisation of the perovskite-related cuprate phases $\text{YSr}_2\text{Cu}_2\text{MO}_7+y$ (M = Co, Fe) for potential use as solid oxide fuel cell cathode materials, *J. Mater. Chem* 2005; 15: 2321.
<https://doi.org/10.1039/b502641e>
- [16] J. SANSOM, Perovskite related cuprate phases as potential cathode materials for solid oxide fuel cells, *Solid State Ionics*. 2004; 175: 99-102.
<https://doi.org/10.1016/j.ssi.2004.09.035>
- [17] G. Cordaro, A. Flura, A. Donazzi, R. Pelosato, F. Mauvy, C. Cristiani, G. Dotelli, JC. Grenier, Electrochemical characterization of $\text{PrBa}_2-x\text{Sr}_x\text{Cu}_3\text{O}_{6+\delta}$ layered oxides as innovative and efficient oxygen electrode for IT-SOFCs, *Solid State Ionics* 2020; 348: 115286.
<https://doi.org/10.1016/j.ssi.2020.115286>
- [18] V. Petříček, M. Dušek, L. Palatinus, Crystallographic Computing System JANA2006: General features, *Zeitschrift Für Krist. - Cryst. Mater* 2014; 229.
<https://doi.org/10.1515/zkri-2014-1737>
- [19] <http://www.inls.cnpem.br/linhas-de-luz/xpd-en/overview>, (n.d.). <http://www.inls.cnpem.br/linhas-de-luz/xpd-en/overview/>.
- [20] R. von D. Larson, A. General structure analysis system (GSAS), LAUR 2004; 86-748.
- [21] BH. Toby, EXPGUI, a graphical user interface for GSAS, *J. Appl. Crystallogr* 2001; 34: 210-213.
<https://doi.org/10.1107/S0021889801002242>
- [22] L. Baque, E. Djurado, C. Rossignol, D. Marinha, A. Caneiro, A. Serquis, Electrochemical Performance of Nanostructured IT-SOFC Cathodes with Different Morphologies, in: *ECS Trans.*, ECS, 2009; pp. 2473-2480.
<https://doi.org/10.1149/1.3205802>
- [23] L. Baqué, A. Caneiro, MS. Moreno, A. Serquis, High performance nanostructured IT-SOFC cathodes prepared by novel chemical method, *Electrochem. Commun* 2008; 10: 1905-1908.
<https://doi.org/10.1016/j.elecom.2008.10.010>
- [24] F. Prado, A. Caneiro, A. Serquis, High temperature thermodynamic properties, orthorhombic/tetragonal transition and phase stability of $\text{GdBa}_2\text{Cu}_3\text{O}_y$ and related R123 compounds, *Phys. C Supercond* 1998; 295: 235-246.
[https://doi.org/10.1016/S0921-4534\(97\)01797-8](https://doi.org/10.1016/S0921-4534(97)01797-8)
- [25] A. Jun, J. Kim, J. Shin, G. Kim, Perovskite as a Cathode Material: A Review of its Role in Solid-Oxide Fuel Cell Technology, *Chem Electro Chem* 2016; 3: 511-530.
<https://doi.org/10.1002/celec.201500382>
- [26] X. Xu, J. Guo, Y. Wang, A. Sozzi, Synthesis of nanoscale superconducting YBCO by a novel technique, *Phys. C Supercond.* 2002; 371: 129-132.
[https://doi.org/10.1016/S0921-4534\(01\)01073-5](https://doi.org/10.1016/S0921-4534(01)01073-5)
- [27] U. Anselmi-Tamburini, P. Ghigna, G. Spinolo, G. Flor, Solid state synthesis of $\text{YBa}_2\text{Cu}_3\text{O}_{7-x}$: Mechanisms of BaCuO_2 formation, *J. Phys. Chem. Solids* 1991; 52: 715-721.
[https://doi.org/10.1016/0022-3697\(91\)90173-W](https://doi.org/10.1016/0022-3697(91)90173-W)
- [28] H. Sözeri, H. Özkan, N. Ghazanfari, Properties of YBCO superconductors prepared by ammonium nitrate melt and solid-state reaction methods, *J. Alloys Compd* 2007; 428: 1-7.
<https://doi.org/10.1016/j.jallcom.2006.03.038>
- [29] A. Williams, GH. Kwei, RB. Von Dreele, ID. Raistrick, DL. Bish, Joint x-ray and neutron refinement of the structure of superconducting $\text{YBa}_2\text{Cu}_3\text{O}_{7-x}$, *Phys. Rev. B* 1988; 37: 7960-7962.
- [30] P. Benzi, E. Bottizzo, N. Rizzi, Oxygen determination from cell dimensions in YBCO superconductors, *J. Cryst. Growth* 2004; 269: 625-629.
<https://doi.org/10.1016/j.jcrysgro.2004.05.082>
- [31] JD. Jorgensen, MA. Beno, DG. Hinks, L. Soderholm, KJ. Volin, RL. Hitterman, JD. Grace, IK. Schuller, CU. Segre, K. Zhang, M.S. Kleefisch, Oxygen ordering and the orthorhombic-to-tetragonal phase transition in $\text{YBa}_2\text{Cu}_3\text{O}_{7-x}$, *Phys. Rev. B* 1987; 36: 3608-3616.
- [32] JD. Jorgensen, BW. Veal, AP. Paulikas, LJ. Nowicki, GW. Crabtree, H. Claus, WK. Kwok, Structural properties of oxygen-deficient $\text{YBa}_2\text{Cu}_3\text{O}_{7-x}$, *Phys. Rev. B* 1990; 41: 1863-1877.
- [33] Y. Kubo, Y. Nakabayashi, J. Tabuchi, T. Yoshitake, A. Ochi, K. Utsumi, H. Igarashi, M. Yonezawa, Determination of the orthorhombic-tetragonal $\text{YBa}_2\text{Cu}_3\text{O}_{7-\delta}$ phase boundary in the δ -T diagram, *Jpn. J. Appl. Phys* 1987; 26: L1888-L1891.
<https://doi.org/10.1143/JJAP.26.L1888>
- [34] J. Mizusaki, H. Tagawa, K. Hayakawa, K. Hirano, Thermal Expansion of $\text{YBa}_2\text{Cu}_3\text{O}_{7-x}$ as Determined by High-Temperature X-ray Diffraction under Controlled Oxygen Partial Pressures, *J. Am. Ceram. Soc* 1995; 78: 1781-1786.
<https://doi.org/10.1111/j.1151-2916.1995.tb08889.x>
- [35] M. Truchlý, T. Plecenik, O. Krško, M. Gregor, L. Satrapinskyy, T. Roch, B. Grančič, M. Mikula, A. Dujavová, Š. Chromik, P. Kúš, A. Plecenik, Studies of $\text{YBa}_2\text{Cu}_3\text{O}_{6+x}$ degradation and surface conductivity properties by Scanning Spreading Resistance Microscopy, *Phys. C Supercond* 2012; 483: 61-66.
<https://doi.org/10.1016/j.physc.2012.07.004>
- [36] W. SUKSAMAI, I. METCALFE, Measurement of proton and oxide ion fluxes in a working Y-doped BaCeO_3 SOFC, *Solid State Ionics* 2007; 178: 627-634.
<https://doi.org/10.1016/j.ssi.2007.02.003>
- [37] T. Sakai, S. Matsushita, J. Hyodo, Y. Okuyama, M. Matsuka, T. Ishihara, H. Matsumoto, Effect of doped ceria interlayer on cathode performance of the electrochemical cell using proton conducting oxide, *Electrochim. Acta* 2012; 75: 179-184.
<https://doi.org/10.1016/j.electacta.2012.04.102>
- [38] J. Lagaeva, D. Medvedev, A. Demin, P. Tsiakaras, Insights on thermal and transport features of $\text{BaCe}_{0.8}\text{-Zr}_{0.2}\text{O}_{3-\delta}$ proton-conducting materials, *J. Power Sources* 2015; 278: 436-444.
<https://doi.org/10.1016/j.jpowsour.2014.12.024>
- [39] T. Ohzeki, S. Hasegawa, M. Shimizu, T. Hashimoto, Analysis of phase transition behavior of BaCeO_3 with thermal analyses and high temperature X-ray diffraction, *Solid State Ionics* 2009; 180: 1034-1039.
<https://doi.org/10.1016/j.ssi.2009.05.019>

- [40] A. Donazzi, R. Pelosato, G. Cordaro, D. Stucchi, C. Cristiani, G. Dotelli, I.N. Sora, Evaluation of Ba deficient $NdBaCo_2O_{5+\delta}$ oxide as cathode material for IT-SOFC, *Electrochim. Acta* 2015; 182: 573-587.
<https://doi.org/10.1016/j.electacta.2015.09.117>

Received on 15-07-2021

Accepted on 05-09-2021

Published on 26-09-2021

DOI: <https://doi.org/10.15377/2410-4701.2021.08.10>

© 2021 Grassi *et al.*; Zeal Press.

This is an open access article licensed under the terms of the Creative Commons Attribution Non-Commercial License (<http://creativecommons.org/licenses/by-nc/3.0/>) which permits unrestricted, non-commercial use, distribution and reproduction in any medium, provided the work is properly cited.